

Supporting Information

**Antenna-Enhanced Triplet-State Emission of
Individual Mononuclear
Ruthenium-(II)-Bis-terpyridine Complexes
Reveals Their Heterogeneous Photophysical
Properties in the Solid State**

Janning F. Herrmann,^{†,‡} Paul S. Popp,^{†,‡} Andreas Winter,^{†,¶} Ulrich S.
Schubert,^{†,¶} and Christiane Höppener^{*,†,‡}

NanoBioPhotonics Group, WWU Münster, Germany

E-mail: christiane.hoepfener@wwu.de

*To whom correspondence should be addressed

[†]NanoBioPhotonics Group, WWU Münster, Germany

[‡]Physikalisches Institut, Westfälische Wilhelms-Universität Münster, Wilhelm-Klemm-Str. 10,
48149 Münster, Germany

[¶]Laboratory for Organic and Macromolecular Chemistry (IOMC), Friedrich Schiller University Jena,
Humboldtstr. 10, 07743 Jena, Germany and Center for Energy and Environmental Chemistry Jena
(CEEC Jena) Jena, Philosophenweg 7a, 07743 Jena, Germany

Sample Preparation

Samples prepared according to the preparation protocol given in the *Materials and Methods* section were characterized for their surface roughness and film thickness by means of conventional atomic force microscopy (AFM). Figure SI-1 displays a typical topography image. The scratch in the film was carefully applied with a sharp razor edge. Aside the groove the PMMA film is smooth and reveals a surface roughness comparable to the one of cleaned glass coverslip. Partly, small aggregations are observed caused by the removal of PMMA from the groove region. The groove depth was measured at different positions and yields 1.5 nm - 2 nm.

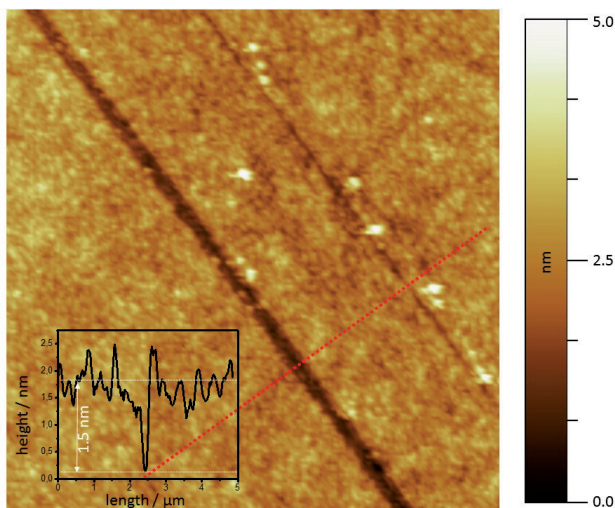


Figure SI-1: Atomic Force Microscopy (AFM) image of the PMMA layer. The topography scan taken in the region of the scratch identifies a groove in the PMMA layer due to razor edge scratching. Inset: Line-profile taken along the red line revealing the depth of the grooves.

Confocal and Antenna-enhanced Microscopy and Spectroscopy

In addition to the description of the setup in the *Materials and Methods* section a schematic representation is displayed in SI-2.

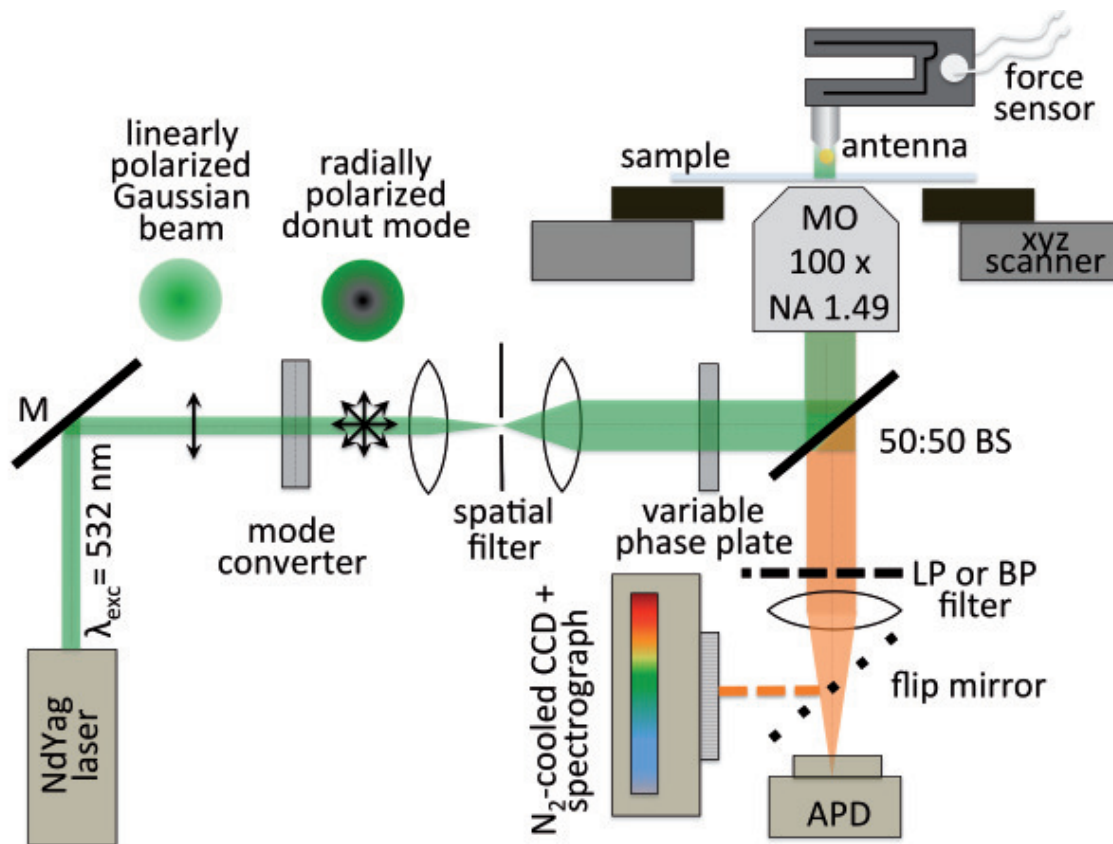


Figure SI-2: Schematic outline of the experimental setup for the confocal and antenna-enhanced phosphorescence investigations. Abbreviations: M-mirror, BS- beam splitter, LP- long-pass filter, BP -band-pass filter, MO - microscope objective, FM - flip mirror

For comparison, additional spectra taken on $\text{Ru}^{2+}[\text{L}]_2(\text{PF}_6^-)_2$ complexes with an expected emission peak at 660 nm are displayed in Figure SI-3. The emission peak varies slightly across the shown spectral region and is found to be centered at $\lambda_{phos} \approx 660 \text{ nm}$ ($\pm 25 \text{ nm}$). The phosphorescence is characterized by a broad emission peak (FWHM $\approx 100 \text{ nm}$). Due to ensemble averaging the profiles reveal only a faint asymmetry, which is ascribed to vibronic progressions centered about 60 nm on the long wavelength tail of the main peak.

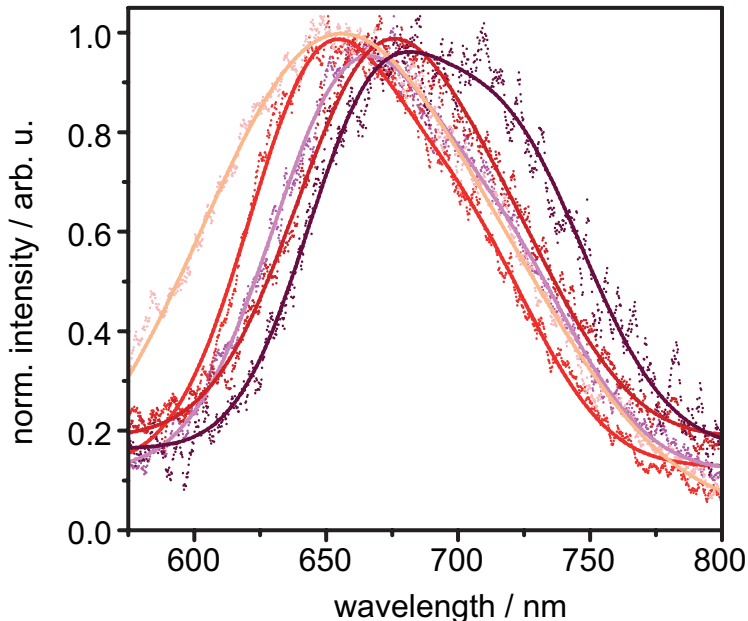


Figure SI-3: Typical phosphorescence spectra of red-emitting $\text{Ru}^{2+}[\text{L}]_2(\text{PF}_6^-)_2$ prepared in a thin film. Coordination complexes are excited with a radially polarized laser with an emission wavelength of 532 nm (± 10 nm) and an excitation power of 1 μW .

Single-molecule emission spectra of the subset of $\text{Ru}^{2+}[\text{L}]_2(\text{PF}_6^-)_2$ with a blue-shifted emission from 660 nm are shown in Figure SI-4. Similarly to the spectra shown in Figure SI-3 the spectral position varies. Typically, the luminescence emission is observed across a spectral range of ~ 540 nm to 620 nm. Clearly the spectra display a double peak structure. In accordance with a two-state model the short wavelength peak (main peak) shows an asymmetry. The second peak is assigned to vibronic progressions.

Confocal luminescence decay spectra of both subsets were acquired to verify that the lifetime of these $\text{Ru}^{2+}[\text{L}]_2(\text{PF}_6^-)_2$ complexes is on the order of nanoseconds (Figure SI-5A). Therefore, it can be excluded, that the excitation conditions lead to a saturation of potentially long-lived (i.e. $\sim \mu\text{s}$) excited states leading to a low photon count rate for the red-emitting complexes in the confocal and antenna-enhanced measurements. Spectrally correlated decay measurements show different lifetimes for the identified subsets of $\text{Ru}^{2+}[\text{L}]_2(\text{PF}_6^-)_2$ complexes. For the red-emitting $\text{Ru}^{2+}[\text{L}]_2(\text{PF}_6^-)_2$ complexes ensemble lifetime measurements were acquired by accumulation of the phosphorescence signal whilst

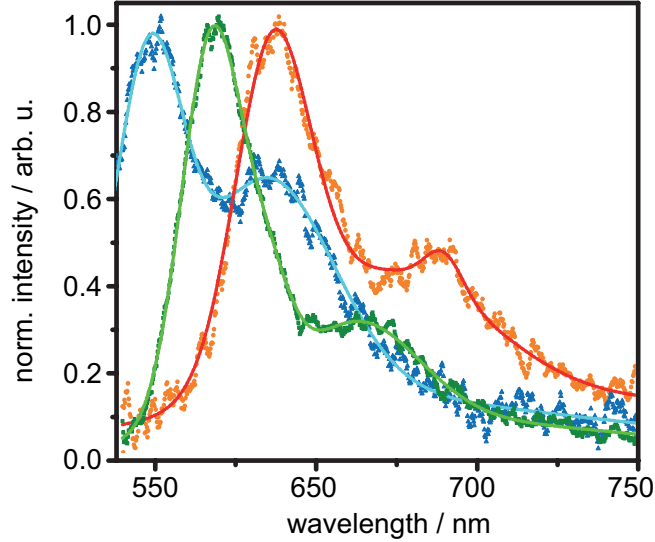


Figure SI-4: Typical emission spectra of $\text{Ru}^{2+}[\text{L}]_2(\text{PF}_6^-)_2$ prepared in a thin film with a blue shifted emission compared to the expected emission spectrum. Coordination complexes are excited with a radially polarized laser with an emission wavelength of 532 nm (± 10 nm) and an excitation power of 1 μW .

slowly scanning an area of $5 \times 5 \mu\text{m}^2$. This region showed a homogenous phosphorescence emission centered at ~ 660 nm. The corresponding decay curve (red curve, Figure SI-5B) follows a bi-exponential decay with lifetimes of $\tau_1 = 4.5$ ns (± 0.1 ns) and $\tau_2 = 42$ ns (± 0.5 ns). The latter state lifetime coincides with the one determined from concentrated $\text{Ru}^{2+}[\text{L}]_2(\text{PF}_6^-)_2$ solutions. In accordance with the observed fluctuations in the intrinsic quantum yield of both $\text{Ru}^{2+}[\text{L}]_2(\text{PF}_6^-)_2$ complex subsets, the lifetime of the complexes with a blue-shifted emission is shortened. The luminescence decay curves are acquired on individual complexes and thus, follow a mono-exponential profile. An average excited state lifetime of 3.3 ns (± 0.6 ns) is found for this subset (s.f. Figure SI-5B). Therefore, the bi-exponential decay of the red-emitting entities can be assigned to a few $\text{Ru}^{2+}[\text{L}]_2(\text{PF}_6^-)_2$ complexes with a blue-shifted emission profile yielding a decay time of 4.5 ns and a large number of red-emitting $\text{Ru}^{2+}[\text{L}]_2(\text{PF}_6^-)_2$ complexes with a significant extended excited state lifetime.

$\text{Ru}^{2+}[\text{L}]_2(\text{PF}_6^-)_2$ complexes with a main peak centered at ~ 580 nm often show luminescence intermittency on different time scales. Figure SI-6 shows a typical time trajectory.

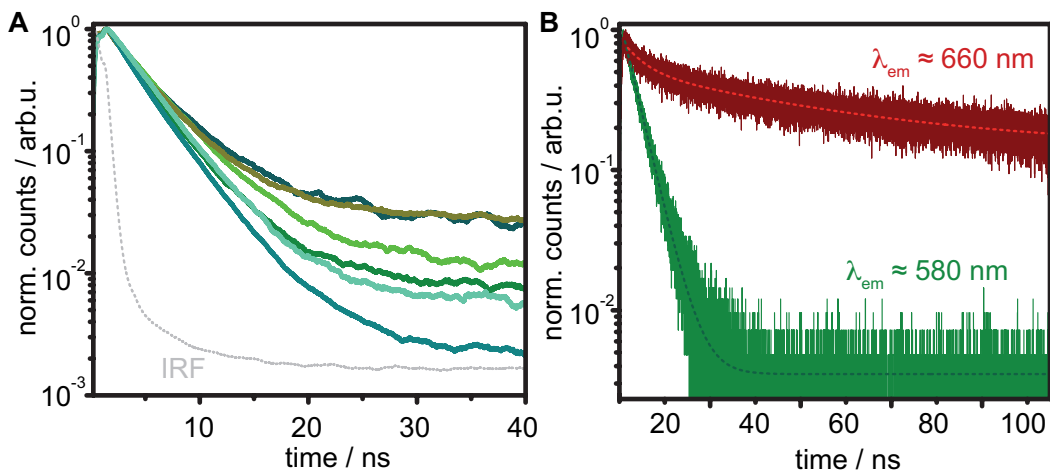


Figure SI-5: Confocal luminescence decay spectra of $\text{Ru}^{2+}[\text{L}]_2(\text{PF}_6^-)_2$ prepared in a thin film. (A) Measurements taken on individual complexes. (B) Spectrally correlated decay curves. The green spectrum corresponds to a single $\text{Ru}^{2+}[\text{L}]_2(\text{PF}_6^-)_2$ with a blue shifted emission compared to the expected emission spectrum. The green solid line shows a fit with a monoexponential decay and a lifetime of 3.8 ns. The red phosphorescence decay spectrum is acquired over a large number of $\text{Ru}^{2+}[\text{L}]_2(\text{PF}_6^-)_2$ complexes with a peak emission at ~ 660 nm. The solid line shows a corresponding fit with a bi-exponential decay leading to lifetimes of 4.5 ns and 42 ns.

The observed off-time periods are indicative for an intermolecular coupling to non-radiative states ($^{\text{HS}}$ dd-state, or more likely to the long-lived T1 state and possibly to the MLCT' state). Due to the density of complexes within the sample, intramolecular coupling to non-radiative states of complexes with common emission properties ($\lambda_{\text{em}} \approx 660$ nm) may also cause quenching of the luminescence emission.

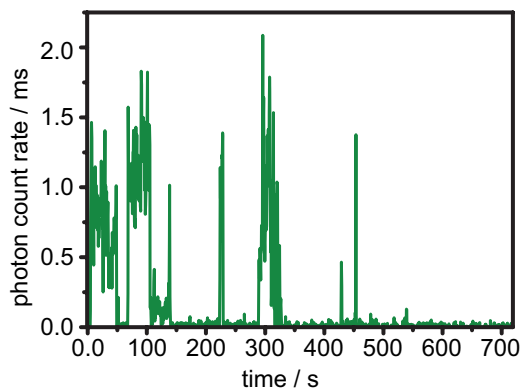


Figure SI-6: Emission time trajectory of a blue-emitting $\text{Ru}^{2+}[\text{L}]_2(\text{PF}_6^-)_2$ reveals emission intermittency.

Analytical solutions of the molecular transition rates

For quantitative comparison of the spontaneous emission enhancement as a function of the antenna-complex separation and the intrinsic quantum yield of the complexes, we follow the established theoretical analysis of the transition rates introduced in references [1,2]. The theoretical model accomplished for a spherical nanoparticle antenna considers a two level system located at r_o . In this case, the excitation rate is proportional to the absolute square of the excitation field E along the direction of the absorption dipole moment μ in the environment of the two level system and thus, given by $\gamma_{exc} \propto |\mu E(r_o)|^2$. The spontaneous decay rate from the excited state of lowest energy $E_i = \hbar\omega_i$ to the ground states with a final energy $E_g = \hbar\omega_g$ is derived from Fermi's golden rule and thus, yields

$$\gamma = (\pi\omega)/(3\hbar\epsilon_o) |\mu|^2 \cdot \rho(r_o, \omega) = 6\omega/(\pi c^2)(n_\mu \text{Im}[\overleftrightarrow{G}(r_o; r_o, \omega)])$$

with ρ denoting the partial local density of states and ω is the difference of the angular frequencies of the involved excited and ground states ($\omega = \omega_i - \omega_g$).

Based on the the Green's formalism the partial density of local states is expressed by the dyadic Green's function \overleftrightarrow{G} which is the sum of the Green's function in free space and the scattering environment, here, the metallic nanostructure in the form of a spherical AuNP. In the dipolar approximation limit the AuNP can be considered as a dipole located at the center of the AuNP (r_m). Hence, the field at r emitted by the quantum emitter in the presence of the spherical nanoparticle antenna is determined by $E(r) = \omega^2/(\epsilon_o c^2) \cdot \overleftrightarrow{G}(r, r_o) \cdot \mu$, and thus, leads to $\overleftrightarrow{G}(r, r_o) = \overleftrightarrow{G}_o(r, r_o) + \omega^2/(\epsilon_o c^2) \overleftrightarrow{G}_o(r, r_m) \alpha_{eff} \overleftrightarrow{G}_o(r_m, r_o)$ with α_{eff} being the effective polarizability, which accounts for the quasi-static polarizability α and for radiation dampening. For a spherical nanoparticle α is given by $\alpha = 4\pi\epsilon_o D/2 \cdot [(\epsilon_{NP} - \epsilon_{sur})/(\epsilon_{NP} + 2\epsilon_{sur})]$.

Taking into account that the normalized radiated power P/P_o is identical to the radiative rate enhancement $\gamma_{rad}/\gamma_{rad}^o$ integration of $|E^2|$ over a surface enclosing dipole of the quantum emitter and the spherical antenna yields for the radiative rate enhancement:

$$\gamma_{rad}/\gamma_{rad}^o = \left| 1 + c_2(\omega_{rad}(\omega_{rad})) \cdot \frac{R^3}{R+z^3} \right|^2$$

$$\text{with } c_1(\omega_{rad}) = [\epsilon_{NP}(\omega_{rad}) - \epsilon_{sur}(\omega_{rad})]/[\epsilon_{NP}(\omega_{rad}) + 2\epsilon_{sur}(\omega_{rad})].$$

Similarly the exception rate enhancement can be determined, and according to reciprocity, yields an identical expression to $\gamma_{rad}/\gamma_{rad}^o$:

$$\gamma_{exc}/\gamma_{exc}^o = \left| 1 + c_2(\omega_{exc}) \cdot \frac{R^3}{R+z^3} \right|^2$$

$$\text{with } c_1(\omega_{exc}) = [\epsilon_{NP}(\omega_{exc}) - \epsilon_{sur}(\omega_{exc})]/[\epsilon_{NP}(\omega_{exc}) + 2\epsilon_{sur}(\omega_{exc})].$$

Since the nanoparticle antenna opens up a new dissipation channel, relaxation of the excited state involves also non-radiative transition to electromagnetic modes of the metal nanoparticle. To a first approximation the nanoparticle interface can be considered as a plane interface acting as a mirror substrate. Therefore, a virtual dipole is induced in the metal interface. Taking into account Poynting's theorem and the polarization current $j = -i\omega\mu\delta(r - r_o)$ induced by the local field, the absorption rate due to the metal interface normalized to the radiated yield can be calculated:

$$\gamma_{abs}/\gamma_{rad}^o = c_3(\omega_{rad}) \cdot \frac{1}{(k \cdot z)^3}$$

$$\text{with } c_3(\omega_{rad}) = 3/4Im[\epsilon_{NP}(\omega_{exc}) - \epsilon_{sur}(\omega_{rad})]/[\epsilon_{NP}(\omega_{rad}) + \epsilon_{sur}(\omega_{rad})].$$

The obtained analytical solutions clearly show different dependencies on the antenna-quantum emitter separation. Further, the expression for $\gamma_{exc}/\gamma_{exc}^o$, $\gamma_{rad}/\gamma_{rad}^o$ and $\gamma_{abs}/\gamma_{rad}^o$ reveal characteristic wavelength dependencies, which cause the enhancement of the spontaneous emission rate to be detuned from the plasmon resonance of the spherical AuNPs. In case of $\gamma_{abs}/\gamma_{rad}^o$ higher order correction terms can be derived accounting for deviations from the dipolar approximation limit [3]. Losses in the metal interface due to the radiating dipole are caused by the excitation of non-radiative surface plasmon modes. These analytical solu-

tions for the corresponding transition rates allow for a quantitative analysis of the distance dependence and quantum yield dependence of the spontaneous emission rates in the case of molecules oriented with their transition dipole moment vertically to the surface. These can be identified in the confocal and antenna-enhanced images using a radially polarized laser beam for their irradiation circular single spot emission pattern (s.f. Figure 2C)).

References

- [1] Bharadwaj, P.; Anger, P.; Novotny, L. Nanoplasmonic enhancement of single-molecule fluorescence. *Nanotechnology* 2007, 18, 044017.
- [2] Bharadwaj, P.; Deutsch, B.; Novotny, L. Optical Antennas. *Adv. Opt. Photonics* 2009,1, 438-483.
- [3] Klimov, V.; Letokhov, V. Electric and magnetic dipole transitions of an atom in the presence of spherical dielectric interface. *Laser Phys.* 2005, 15, 61-73.